Available online at www.sciencedirect.com
SCIENCE DIRECT®
Journal of Structural Biology 149 (2005) 191–203
Journal of Structural Biology
www.elsevier.com/locate/yjsbi

Structural characterization of components of protein assemblies by comparative modeling and electron cryo-microscopy

Maya Topf[a], Matthew L. Baker[b], Bino John[c], Wah Chiu[b], Andrej Sali[a,*]

[a] *Departments of Biopharmaceutical Sciences and Pharmaceutical Chemistry, California Institute for Quantitative Biomedical Research, Mission Bay Genentech Hall, 600 16th Street, Suite N472D, University of California, San Francisco, CA 94143, USA*
[b] *Verna and Marrs McLean Department of Biochemistry and Molecular Biology, National Center for Macromolecular Imaging, Baylor College of Medicine, One Baylor Plaza, Houston, TX 77030, USA*
[c] *Memorial Sloan-Kettering Cancer Center, 1275 York Avenue, New York, NY 10021, USA*

Received 13 August 2004, and in revised form 5 November 2004
Available online 8 December 2004

Abstract

We explore structural characterization of protein assemblies by a combination of electron cryo-microscopy (cryoEM) and comparative protein structure modeling. Specifically, our method finds an optimal atomic model of a given assembly subunit and its position within an assembly by fitting alternative comparative models into a cryoEM map. The alternative models are calculated by MODELLER [J. Mol. Biol. 234 (1993) 313] from different sequence alignments between the modeled protein and its template structures. The fitting of these models into a cryoEM density map is performed either by FOLDHUNTER [J. Mol. Biol. 308 (2001) 1033] or by a new density fitting module of MODELLER (Mod-EM). Identification of the most accurate model is based on the correlation between the model accuracy and the quality of fit into the cryoEM density map. To quantify this correlation, we created a benchmark consisting of eight proteins of different structural folds with corresponding density maps simulated at five resolutions from 5 to 15 Å, with three noise levels each. Each of the proteins in the set was modeled based on 300 different alignments to their remotely related templates (12–32% sequence identity), spanning the range from entirely inaccurate to essentially accurate alignments. The benchmark revealed that one of the most accurate models can usually be identified by the quality of its fit into the cryoEM density map, even for noisy maps at 15 Å resolution. Therefore, a cryoEM density map can be helpful in improving the accuracy of a comparative model. Moreover, a pseudo-atomic model of a component in an assembly may be built better with comparative models of the native subunit sequences than with experimentally determined structures of their homologs.

Keywords: Protein structure prediction; Comparative modeling; Electron cryo-microscopy; Fitting

1. Introduction

The native structures of the individual proteins do not yield the "full picture" of the functional assemblies, such as viruses, ion channels, ribosomes, proteasomes, and other molecular machines (Alberts, 1998; Russell et al., 2004; Sali et al., 2003). To this end, the structures of whole assemblies are needed. One of the methods that can be applied to structural characterization of whole assemblies is electron cryo-microscopy (cryoEM) of single particles. Single-particle cryoEM can determine the structures of macromolecular complexes with molecular weights larger than approximately 150 kDa in different functional states and at increasingly higher resolutions (Frank, 2002; Ludtke et al., 2004; Zhou and Chiu, 2003). It is anticipated that the resolution of many single-particle cryoEM structures determined in the immediate future will be in the range of 5–10 Å.

* Corresponding author. Fax: +1 415 514 4231.
E-mail address: sali@salilab.org (A. Sali).
URLs: http://salilab.org, http://ncmi.bcm.tmc.edu/cbs.

1047-8477/$ - see front matter © 2004 Elsevier Inc. All rights reserved.
doi:10.1016/j.jsb.2004.11.004

While it is almost impossible to determine an atomic model only from density maps at 5–10 Å resolution, a wealth of information, such as spatial organization of domains, locations of long α-helices and large β-sheets (Jiang et al., 2001) as well as macromolecular dynamics (Ming et al., 2002; Tama et al., 2002; Wang et al., 2004), can still be obtained from such maps (Russell et al., 2004). Moreover, it has been shown that docking atomic-resolution structures of individual subunits into a cryoEM density map of the intact assembly can result in a useful pseudo-atomic model of the whole assembly (Zhou et al., 2001). Such models can yield significant insights into the structure and function of single proteins and their complexes (Golas et al., 2003; Kostyuchenko et al., 2003; Shin et al., 2003).

Manual docking tools (Beckmann et al., 2001; Beroukhim and Unwin, 1995; Hewat et al., 1998; Hoenger et al., 1998; Rayment et al., 1993; Sosa et al., 1997; Spahn et al., 2001; Voges et al., 1994), which are limited by the experience of the user, are slowly being replaced by more robust and objective docking strategies (Roseman, 2000; Wriggers and Chacon, 2001). The most widely used approach relies on a systematic maximization of the cross-correlation between the model density and the density map. In some earlier studies, this method was employed for local rigid-body refinements of the manual docking solutions, in both reciprocal space (Cheng et al., 1995; Hewat and Blaas, 1996; Kolatkar et al., 1999; Wikoff et al., 1994) and real space (Grimes et al., 1997; Stewart et al., 1993). Recently, routines that rely on a more thorough search over three translational and three rotational degrees of freedom in real space have been introduced, including COAN (Volkmann and Hanein, 1999), DOCKEM (Roseman, 2000), EMFIT (Rossmann, 2000), COLORES (Chacon and Wriggers, 2002; Wriggers et al., 1999), FOLDHUNTER (Jiang et al., 2001), the grid-threading Monte Carlo method (Wu et al., 2003), and 3SOM (Ceulemans and Russell, 2004).

Unfortunately, experimentally determined atomic-resolution structures of the isolated subunits in the complexes are frequently not available. In addition, even if they are available, the induced fit may severely limit their utility in the reconstruction of the whole assembly. In such cases, it might be possible to obtain useful models of the subunits in the correct structural state by comparative protein structure modeling (Baker and Sali, 2001; Jacobson and Sali, 2004; Marti-Renom et al., 2000). For example, partial pseudo-atomic models of the whole yeast (Beckmann et al., 2001; Spahn et al., 2001) and *Escherichia coli* ribosomes (Gao et al., 2003) were obtained by fitting into cryoEM maps comparative protein models calculated from the crystallographic structures of the prokaryotic ribosomal subunits.

Comparative modeling predicts the structure of a target protein sequence by (i) finding one or more related proteins with known structures (i.e., templates), (ii) aligning the target sequence to the template structure, (iii) building a model based primarily on the alignment from the previous step, and (iv) assessing the model (Marti-Renom et al., 2000). It is becoming increasingly applicable and accurate, in large part because of the structural genomics initiative. The structural genomics initiative aims to solve the structures of most protein families by X-ray crystallography or NMR spectroscopy, such that most of the remaining proteins can be modeled with useful accuracy based on their similarity to the known structures (Baker and Sali, 2001; Marti-Renom et al., 2000; Pieper et al., 2004; Sali and Kuriyan, 1999). The largest errors in comparative models result from incorrect sequence alignment and fold assignment, especially in models of the sequences that are only remotely related to their templates (i.e., at less than 30% sequence identity). Most pairs of detectably related protein sequences and structures are currently related at less than 30% sequence identity, with correspondingly large alignment errors (i.e., >20% of misaligned residues). Other errors include rigid-body shifts, errors in the modeling of loops, and errors in side-chain packing (Marti-Renom et al., 2000). It is usually possible to generate a set of models based on alternate templates and alignments that vary in the orientation of domains, packing of secondary structure elements, and conformation of loops. Selecting the best model from a model set can then be attempted through various methods for model assessment (Melo et al., 2002; Sippl, 1993).

Here, we evaluate the utility of cryoEM density maps at 5–15 Å resolution in assessing comparative protein structure models with alignment errors. We describe a method for fitting a given rigid model into a density map, implemented in MODELLER (Sali and Blundell, 1993) (Mod-EM) and an improved version of FOLDHUNTER (Jiang et al., 2003). This procedure is then tested with the aid of a benchmark data set, consisting of eight proteins of different folds with 300 different models each. In addition, we describe the criteria used to assess the correlation between the geometrical accuracy of a model and the quality of its fit into a given density map. Furthermore, we quantify the ability of Mod-EM and FOLDHUNTER to find the most accurate models by the quality of their fit into density maps at different resolutions and noise levels. We also compare model assessment by density fitting with model assessment by statistical potentials of mean force as implemented in the ProsaII program (Sippl, 1993). Finally, we discuss the implications of the results for comparative protein structure modeling and for improving the interpretation of cryoEM density maps.

2. Methods

2.1. Docking a given model into a density map by Mod-EM

A rapid correlation-based method for docking a probe model into a cryoEM density map was implemented in MODELLER-8 (Mod-EM), which will be available soon at http://salilab.org/modeller.

The cryoEM density map is represented by intensities at points on a cubic grid in the X-PLOR format (Brünger, 1992). The spacing between the points on this grid, typically 1 Å, is independent of the map resolution.

Before fitting, the probe model is converted into probe density, $\rho^{\text{probe}}(r)$. Each atom in the probe model can be represented by one of several atomic density functions, including the Gaussian function (Jiang et al., 2003), the hybrid Gaussian/sphere model (Pittet et al., 1999), and the uniform sphere model. All of the tested forms performed similarly in our benchmark (data not shown), thus we only present the results for the simplest model of atomic density, the uniform sphere model:

$$\rho^{\text{probe}}(\vec{r}) = m[f(|\vec{r}-\vec{a}|)], \quad f(|\vec{r}-\vec{a}|) = \begin{cases} 1 & \text{for } |\vec{r}-\vec{a}| \leqslant R, \\ 0 & \text{for } |\vec{r}-\vec{a}| > R, \end{cases} \tag{1}$$

where m is the atomic mass, $\vec{a}$ is the atomic position, $|\vec{r}-\vec{a}|$ is the distance of point $\vec{r}$ from the atomic center, and R is the atomic van der Waals radius (MacKerell et al., 1998). The uniform sphere model of an atom is the sphere of uniform density with the radius equal to the van der Waals radius of the atom.

The best fit between the probe model and the cryoEM density map is obtained by changing the position of the model so as to maximize the cross-correlation between the probe density and the cryoEM density. The cross-correlation is measured by a normalized fitting score:

$$C = \frac{\sum_{i=1}^{M} \rho_i^{\text{EM}} \left(\sum_{j=1}^{N} \rho_{i,j}^{\text{probe}} \right)}{\sqrt{\sum_{i=1}^{M} (\rho_i^{\text{EM}})^2 \sum_{i=1}^{M} \left(\sum_{j=1}^{N} \rho_{i,j}^{\text{probe}} \right)^2}}, \tag{2}$$

where M is the number of grid points in the cryoEM density map covered by the probe density, ρ_i^{EM} is the intensity at grid point i of the cryoEM density map, N is the number of atoms in the probe model, $\rho_{i,j}^{\text{probe}}$ is the atomic density of atom j at grid point i (Eq. (1)), and $\sum_{j=1}^{N} \rho_{i,j}^{\text{probe}}$ is the total probe density at grid point i.

Optionally, the cross-correlation can be approximated by a more computationally efficient un-normalized fitting score:

$$C' = \sum_{j=1}^{N} m_j \rho_i^{\text{EM}}, \tag{3}$$

where N is the number of atoms, ρ_j^{EM} is the cryoEM density at the grid point closest to atom j and m_j is its atomic mass. This approximation requires that the grid spacing for the cryoEM density is smaller than the atomic radii in Eq. (1). This criterion is satisfied here by using the cryoEM density grid spacing of 1 Å.

Three different protocols were implemented for the optimization of the fitting score C in an attempt to balance speed and accuracy of finding a good optimum of C. The first protocol, "center-rotation," is used if the cryoEM map density describes the probe model only (i.e., they have the same size). For example, this condition applies when the probe model corresponds to a large protein or when a density map of a large complex is segmented into subunit maps. The protocol begins by translating the center of mass of the probe model to the center of mass of the cryoEM density map. A search over the three rotational Euler angles (ϕ, θ, ψ) is then performed to maximize C'. The search begins by calculating C' for all combinations of the Euler angles in steps of 30°. Next, the best fit from this coarse search is refined by a finer local search in all three Euler angles. The local refinement is repeated iteratively three times, with the final step of 0.24°. For a protein of 150 residues, the whole calculation typically takes less than 0.5 min on a 3.0 GHz Intel Xeon processor.

The second protocol, "Monte Carlo," is used when the probe model is smaller than the cryoEM density map. This condition applies when the probe model corresponds to one of the molecular components of the complex. The protocol starts with an arbitrary superposition of the probe model and cryoEM densities (typically, superposing their centers of mass), and proceeds by a fixed number of Monte Carlo steps, typically 250–500. A single Monte Carlo step consists of (i) a random translation of the probe for one grid unit of the cryoEM density map, (ii) a search for the three Euler angles that maximize C', using the "center-rotation" protocol described above, and (iii) an application of the Metropolis criterion (Metropolis and Ulam, 1949). For the calculation of the Metropolis criterion, the overlap between the probe model and the cryoEM density map is quantified by C. A typical acceptance rate for these Monte Carlo steps is 15–20% at the temperature of 5000 units. For a probe model of 80–100 residues (32^3 Å^3) and a cryoEM density map of 96^3 Å^3, the calculation takes approximately 1 min.

The third protocol, "scanning Monte Carlo," is used when the probe model is significantly smaller ($\leqslant$35%) than the cryoEM density volume. This condition applies when the probe model corresponds to one of the minor molecular components of the complex. The cryoEM density map is divided into cells similar in volume to the probe. For each such cell, a local search is performed if the randomly oriented probe density centered within the cell has a positive C. The local search starts with

the probe positioned at the center of the cell. The optimal orientations at this position and all 26 (i.e., $3 \times 3 \times 3 - 1$) neighboring grid points are obtained successively by enumerating all three Euler angles as described for the "center-rotation" protocol above. A Monte Carlo criterion is applied to each one of these 27 optimal orientations. Within each cell, such a search is repeated 25–50 times. The calculation typically takes ~10–15 min. When the cryoEM density map covers only the probe model, this protocol can be used for a translational and rotational refinement of the initial superposition of the centers of mass. This calculation typically takes ~1–2 min.

2.2. Improved FOLDHUNTER (FOLDHUNTER.py)

FOLDHUNTER also relies on maximizing the cross-correlation between a probe model and a cryoEM density map (Jiang et al., 2003). The probe model is first transformed into a probe density map, over the same volume as the cryoEM density map regardless of their relative sizes. Next, an exhaustive search of Euler angles is performed at each grid point of the cryoEM density map. Previous versions of FOLDHUNTER successfully fit both X-ray and cryoEM densities into low to intermediate resolution cryoEM densities (Bowman et al., 2003; Jiang et al., 2003; Mao et al., 2004; Zhou et al., 2001). However, that version of FOLDHUNTER depended on separate EMAN programs (Ludtke et al., 1999) for data manipulation. Recently, a faster version of FOLDHUNTER (FOLDHUNTER.py) was implemented. FOLDHUNTER.py performs a coarse initial fit with probe and density maps shrunk by a factor of 2, then produces the final fit by refining the initial solution with the maps at the original size. A typical calculation takes 10 min for a 96^3 Å^3 cryoEM density map on a 3.0 GHz Intel Xeon processor, which is approximately five times faster than the previous versions of FOLDHUNTER. The new version of FOLDHUNTER is available in the AIRS package distributed with EMAN (http://ncmi.bcm.tmc.edu/~stevel/EMAN/doc/).

2.3. The benchmark for testing the fitting programs

We created a benchmark for testing the ability of Mod-EM and FOLDHUNTER to rank a number of probe models of the same protein by their geometrical accuracy. This benchmark consists of eight pairs of proteins of known structure sharing between 12 and 32% sequence identity. Their sizes range from approximately 100 to 300 residues and they represent all of the major fold types (i.e., α, β, α + β, and α/β) (Levitt and Chothia, 1976).

Using the native structure for each of the eight probe proteins, five noiseless cryoEM density maps were simulated at 5, 8, 10, 12, and 15 Å resolution, employing the PDB2MRC and PROC3D programs in EMAN (Ludtke et al., 1999). The exact choice of sample resolutions is not important because the results do not change significantly over a few angstroms. The density map was constructed by summing Gaussian functions for all atoms in the probe protein (Ludtke et al., 1999). The standard deviation (i.e., standard width) of the Gaussian was constant for all atoms, and equal to half of the resolution of the density map. To simulate cryoEM density maps more realistically, two additional sets of maps were calculated with flatband noise at 0.25 σ and 0.75 σ, where σ is the standard deviation of the simulated density map (Ludtke et al., 1999). Thus, the entire benchmark contains 120 simulated cryoEM density maps.

For each of the eight test pairs, 300 alignments spanning approximately 0–100% correctly aligned positions were created by a modified version of MOULDER (John and Sali, 2003). A pair of aligned positions is aligned correctly if they match the structure-based alignment calculated with the program CE (Shindyalov and Bourne, 1998). A single comparative protein structure model of the probe sequence, containing all non-hydrogen atoms, was built for each alignment by MODELLER-6, applying the default model building routine "model" with fast refinement (Sali and Blundell, 1993).

For each of the eight test proteins, an "ideal" model was built based on the structural alignment of the target and the template obtained by the CE program (Shindyalov and Bourne, 1998). The "ideal" models were either identical or very close to the most accurate models in the benchmark of 300 models defined above (the average native overlap for the ideal and most accurate models is 85 and 86%, respectively).

The entire benchmark, including eight pairs of test and template structures, the corresponding 2400 atomic models, and the 120 cryoEM density maps are available at http://salilab.org/modem.

2.4. Assessing model accuracy

Two criteria were used to assess the geometrical accuracy of the models of each protein (John and Sali, 2003; Marti-Renom et al., 2004). First, the root-mean-square (RMS) error between the corresponding Cα atoms in the model and the native structure was calculated upon rigid-body least-squares superposition of all the Cα atoms, as implemented in the SUPERPOSE command of MODELLER. Second, the percentage of structurally equivalent positions was defined as the percentage of the Cα atoms in the model that are within 3.5 Å of the corresponding atoms in the superposed native structure ("native overlap"). The 3.5 Å cutoff value is typically used in evaluation of comparative models (Marti-Renom et al., 2000), including the Critical Assessment of Techniques for Protein Structure Prediction (CASP) (Moult et al., 2003).

In addition, for each of the eight test proteins, their native structure, their template structure, the 300 models, and the "ideal" model were characterized by the optimal fitting scores for the simulated cryoEM maps calculated from their native structures (15 maps in total, one map at each of the five resolutions and three noise levels). The optimal fits were obtained by both Mod-EM ("scanning Monte Carlo" protocol) and FOLDHUNTER.

Finally, all models and native structures were also assessed by a statistical potential *Z*-score, as implemented in the program ProsaII (Sippl, 1993). The *Z*-score is the difference between the statistical potential energy of the model and the mean energy of many unrelated folds onto which the same sequence is "threaded," expressed in units of the standard deviation of the energy distribution. The *Z*-score is proportional to the length of the protein. For most experimentally determined protein structures with ~100 and ~300 residues, the *Z* scores are in the ranges of −8 to −4 and −10 to −6, respectively (Sippl, 1993).

3. Results

Mod-EM and FOLDHUNTER were employed to identify the most accurate comparative models by fitting the alternative models of the same protein into the density maps of their corresponding native structures. The accuracies of the two programs were tested by a benchmark consisting of eight known protein structures with 300 comparative models each. In addition, the accuracy of identifying the most accurate models by a combination of the fitting and ProsaII scores was examined.

3.1. Ranking the models by fitting

As expected, the native structure had the highest fitting score for all proteins at all tested resolutions, with both Mod-EM and FOLDHUNTER (Figs. 1–3). The difference in the fitting scores between the highest scoring model and the native structure was smaller at lower resolutions than at higher resolutions (Fig. 1). For example, for 1DXT, the difference in the Mod-EM fitting scores between the highest scoring model and the native structure was reduced from 0.09 at 8 Å to 0.03 at 12 Å (Fig. 1). For FOLDHUNTER, the corresponding reduction was from 0.10 to 0.06. At a given model accuracy, the fitting score was higher at lower resolution than at higher resolution (Fig. 1), as expected: At a high resolution, only an extremely accurate model will overlap well with the map; at a low resolution, even an inaccurate model will overlap relatively well with the map. For both Mod-EM and FOLDHUNTER, the accuracy of a model was correlated with the fitting score over the whole range of accuracy, at all tested resolutions (5–15 Å) and noise levels (0 σ, 0.25 σ, and 0.75 σ) (Figs. 1–3). For example, for 10 Å cryoEM maps of 1LGA and 1ONC, both fitting methods resulted in a Pearson correlation coefficient ("R^2") between the native overlap and the fitting score that is larger than 0.7 (Fig. 2).

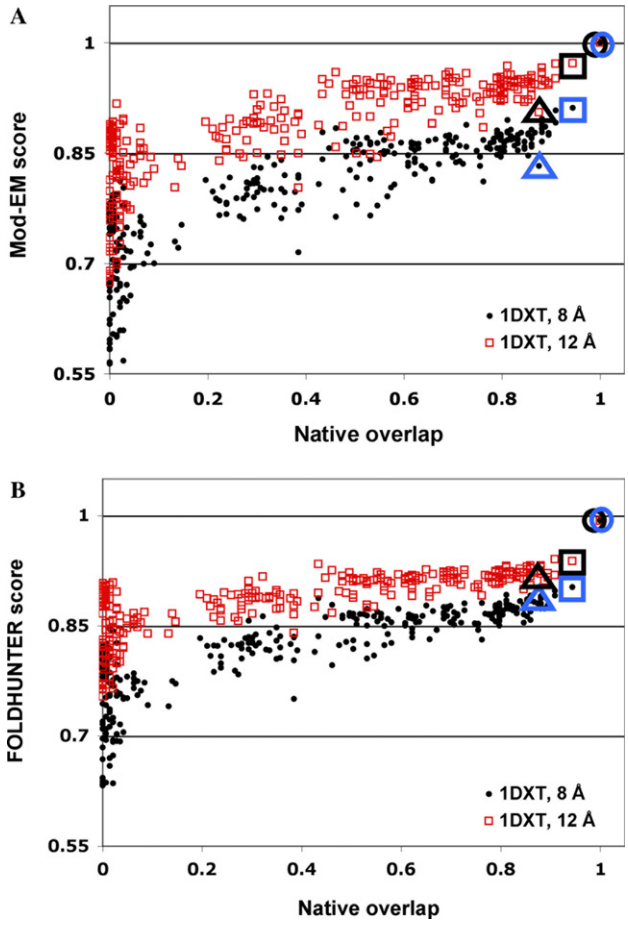

Fig. 1. Fitting of models into the native density maps at different resolutions by Mod-EM (A) and FOLDHUNTER (B). The results are shown for 1DXT at map resolutions of 8 Å (black points) and 12 Å (red squares). The fitting score of the best fit between a probe model and the map is plotted against the native overlap for the native structure (large circle), the 300 comparative models, the template structure (large triangle), and the "ideal" model (large square).

Based on the RMS errors and native overlaps of the most accurate models versus the best-fitting models, both density fitting methods performed similarly in identifying native-like models (Table 1). At sub-nanometer resolutions (5–10 Å), FOLDHUNTER assigned the top score to one of the 15 most accurate models (out of 300) for all eight test proteins, while Mod-EM did so in seven cases. In this resolution range, the average native overlap of the model with the highest Mod-EM fitting score was better than 78%. This value is very close to the best possible native overlap, corresponding to the average native overlap of the most accurate models (i.e., 85%). Even up to 12 Å resolution, the fitting methods selected a model within ~1 Å RMS error of the

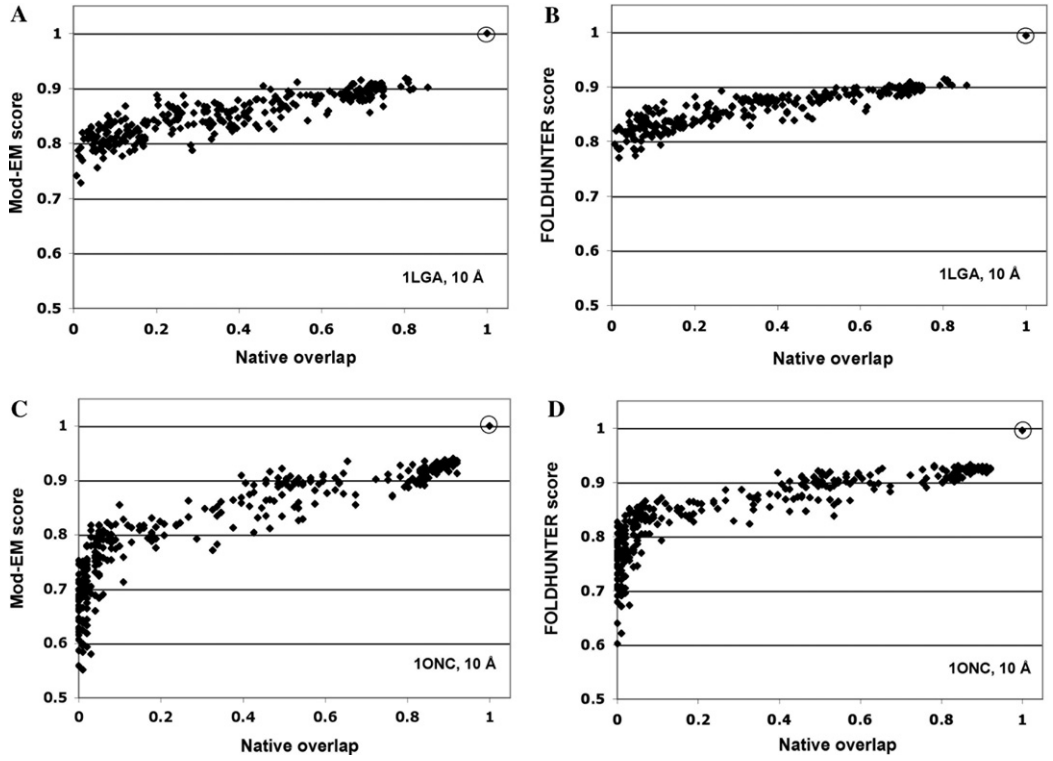

Fig. 2. Fitting of models into the native density map by Mod-EM and FOLDHUNTER. The results are shown for 1LGA (A,B) and 1ONC (C,D). The fitting score of the best fit between a model and the map is plotted against the native overlap for the native structure (encircled) and 300 comparative models. Native density maps at 10 Å resolution without noise were used.

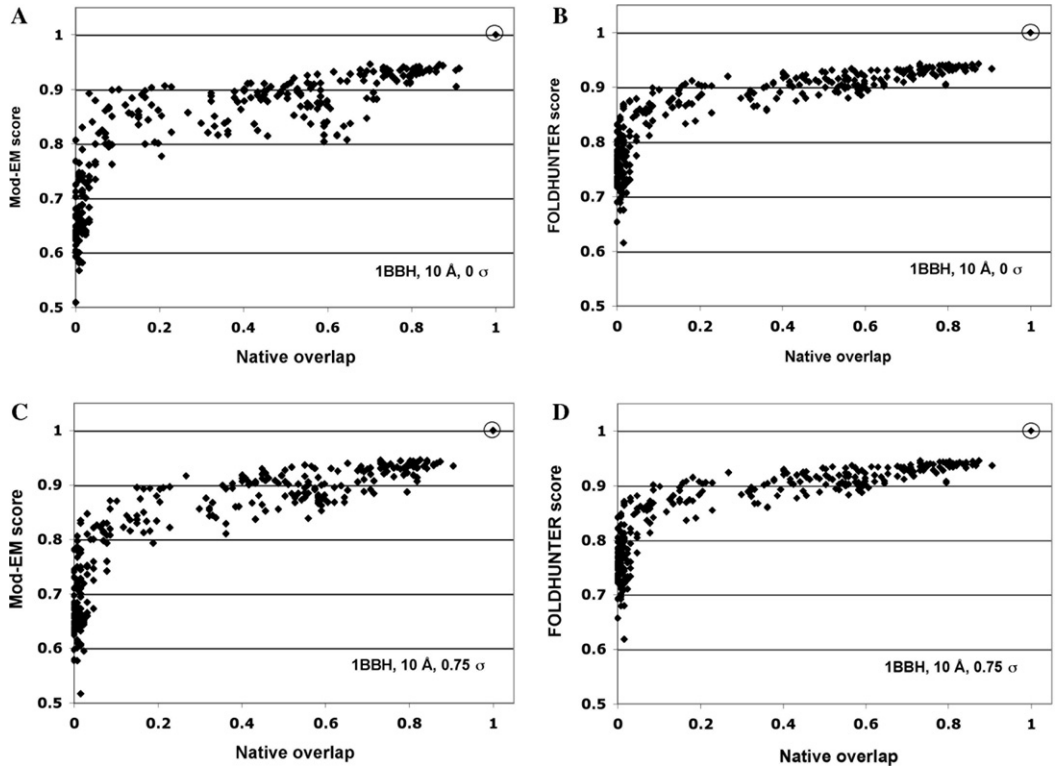

Fig. 3. Fitting of models into the native density maps at different noise levels by Mod-EM (A,C) and FOLDHUNTER (B,D). The results are shown for 1BBH at the map resolution of 10 Å, calculated with two different noise levels: 0 σ (A,B) and 0.75 σ (C,D).

most accurate model in most cases (six and seven of the eight test proteins with Mod-EM and FOLDHUNTER, respectively). In summary, although the fitting does not always identify the most accurate model, the best-fitting model is generally close to the most accurate model.

Mod-EM fitness score identified a more accurate model than the ProsaII statistical potential Z-score for five out of the eight test proteins at sub-nanometer resolution (Table 1). FOLDHUNTER was even more successful, winning over ProsaII in seven cases (data not shown). Even at 15 Å resolution, four of the eight models identified by Mod-EM had a better native overlap than the best model selected by ProsaII (Table 1).

Table 1
Assessing models by fitting into the native density map at sample resolutions

(A) Protein name	RMS error of the most accurate model (Å)	Difference in the RMS errors (Å) between the best-fitting model and the most accurate model						ProsaII
		Noise level (σ)	Resolution of the map (Å)					
			5	8	10	12	15	
Mod-EM								
1CID	3.4	0.00	0.1	0.1	0.1	0.1	0.1	1.2
1MUP	3.3		0.3	2.9	2.9	2.9	10.4	0.7
1LGA	3.2		0.9	0.9	0.9	0.9	0.9	0.0
2CMD	2.5		1.1	0.0	0.0	0.0	0.2	2.8
1DXT	2.0		0.5	0.0	0.0	0.0	0.0	0.6
1BBH	2.5		0.3	0.0	1.1	1.1	1.1	0.1
1ONC	2.2		0.3	0.3	0.3	0.0	0.8	0.4
1C2R	3.4		1.9	0.4	0.2	2.0	2.3	0.2
Average[a]	2.8	0.00	0.7	0.6	0.7	0.9	2.0	0.7
		0.25	0.3	0.6	1.0	1.0	2.0	
		0.75	0.7	0.6	0.8	0.8	2.0	
FOLDHUNTER								
Average[a]	2.8	0.00	0.3	0.3	0.3	1.3	1.6	0.7
		0.25	0.3	0.3	0.5	1.4	1.7	
		0.75	0.3	0.3	0.4	1.4	1.6	
(B) Protein name	Native overlap of the most accurate model	The native overlap of the best-fitting model						ProsaII
		Noise level (σ)	Resolution of the map (Å)					
			5	8	10	12	15	
Mod-EM								
1CID	0.73	0.00	0.69	0.71	0.71	0.71	0.71	0.59
1MUP	0.76		0.74	0.54	0.54	0.54	0.14	0.70
1LGA	0.86		0.80	0.80	0.80	0.80	0.80	0.86
2CMD	0.86		0.81	0.86	0.86	0.86	0.84	0.70
1DXT	0.94		0.91	0.91	0.91	0.91	0.91	0.91
1BBH	0.91		0.80	0.87	0.73	0.73	0.73	0.87
1ONC	0.92		0.89	0.89	0.89	0.91	0.81	0.87
1C2R	0.84		0.68	0.78	0.77	0.66	0.60	0.76
Average	0.85	0.00	0.79	0.80	0.78	0.77	0.69	0.79
		0.25	0.80	0.80	0.76	0.77	0.70	
		0.75	0.79	0.79	0.78	0.77	0.69	
FOLDHUNTER								
Average	0.85	0.00	0.82	0.82	0.81	0.72	0.71	0.79
		0.25	0.82	0.82	0.80	0.72	0.69	
		0.75	0.82	0.82	0.80	0.72	0.70	

The best-fitting model has the highest fitting score with the density map. The most accurate model has the smallest RMS error from the native structure (A) and the highest native overlap (B) among all 300 models in the benchmark. For the ProsaII column, the best model was predicted to be the model with the most significant ProsaII Z-score.

[a] Only the individual data points that lead to the first row of averages in Mod-EM are shown. Individual data points for FOLDHUNTER are not shown.

3.2. Effect of noise

Adding noise to the density maps (at the 0.25 σ and 0.75 σ level) caused a small reduction in the accuracy of the best-fitting model and in the difference between the fitting scores of the highest scoring model and the native structure, but did not affect the results significantly (Fig. 3 and Table 1). For example, the correlation between the native overlaps and the fitting scores of 1BBH was similar at maps with the noise levels of 0 σ and 0.75 σ, for both Mod-EM and FOLDHUNTER (Fig. 3). Both Mod-EM and FOLDHUNTER performed similarly for maps with and without noise (Table 1).

3.3. Fitting the template versus fitting the "ideal" model based on the correct alignment

For the eight probe proteins, the average fitting ranks of the "ideal" models based on best possible alignments (Section 2) are below 18, at sub-nanometer resolutions (Table 2). In contrast, the average fitting ranks of the template structures are above 48. At lower resolutions (i.e., 12 and 15 Å), the template structure is sometimes ranked higher than the "ideal" model, but the average rank of the template is still lower than that of the "ideal" model. For Mod-EM, even at 15 Å resolution, the "ideal" models for seven out of the eight probe proteins are ranked by fitting among the best 50 models; in contrast, five out of the eight template structures are ranked above 100. For example, the "ideal" model of 1DXT and its template structure (1HBG) are ranked 2 and 132, respectively, based on Mod-EM fitting at 8 Å resolution (Fig. 1). At 12 Å resolution, the corresponding ranks are 2 and 139, respectively. Therefore, an accurate comparative model of a protein based on an experimentally determined atomic structure of a remotely related homolog generally fits better into its density map than the homolog itself.

3.4. Composite scoring

Despite the correlation between the fitting score and the ProsaII Z-score (data not shown), these two scores capture different aspects of a model. For example, different models of 1MUP (Fig. 4A) have relatively similar shapes, thus creating difficulties for the fitting score (especially at lower resolution; cf., 1MUP at 15 Å in Table 1), while the statistical potential could still benefit from the different residue accessibilities and pairwise residue distances. On the other hand, different models of 1CID and 2CMD (Fig. 4B) have quite distinct shapes due to the different locations of insertions and deletions, thus allowing the fitting score to perform better than the

Table 2
Assessing the "ideal" model and the template structure by fitting into the target density map

Target—Template	Native overlap of the "ideal" model	Rank of the "ideal" model and the template structure									
		Resolution of the map (Å)									
		5		8		10		12		15	
		Template	"Ideal" model	Template	"Ideal" model	Template	"Ideal" model	Template	"Ideal" model	Template	"Ideal" model
Mod-EM											
1CID—2RHE	0.73	68	15	82	16	101	25	110	32	105	42
1MUP—1RBP	0.76	72	60	69	42	45	27	43	13	15	28
1LGA—2CYP	0.86	9	4	14	30	4	36	5	42	3	50
2CMD—6LDH	0.86	34	1	24	2	5	1	2	1	1	2
1DXT—1HBG	0.94	69	1	132	2	138	1	139	2	143	2
1BBH—2CCY	0.91	34	1	72	3	82	9	94	21	100	23
1ONC—7RSA	0.92	110	3	133	3	136	2	144	1	153	13
1C2R—1YCC	0.86	63	12	93	10	116	13	118	29	129	55
Average	0.86	57	12	77	14	78	14	82	18	81	27
FOLDHUNTER											
1CID—2RHE	0.73	73	16	92	24	66	34	79	50	223	31
1MUP—1RBP	0.76	160	17	229	21	208	57	196	217	141	119
1LGA—2CYP	0.86	42	8	12	15	22	8	42	12	70	12
2CMD—6LDH	0.86	8	1	21	1	14	1	5	4	1	7
1DXT—1HBG	0.94	10	2	18	2	18	1	19	1	12	3
1BBH—2CCY	0.91	4	1	9	2	7	16	12	93	36	104
1ONC—7RSA	0.92	79	2	105	6	104	21	108	27	98	25
1C2R—1YCC	0.86	8	5	31	7	42	7	44	6	44	8
Average	0.86	48	7	65	10	60	18	63	51	78	39

The rank is obtained by sorting the "ideal" model, the template structure, and the 300 comparative models based on their fitting scores.

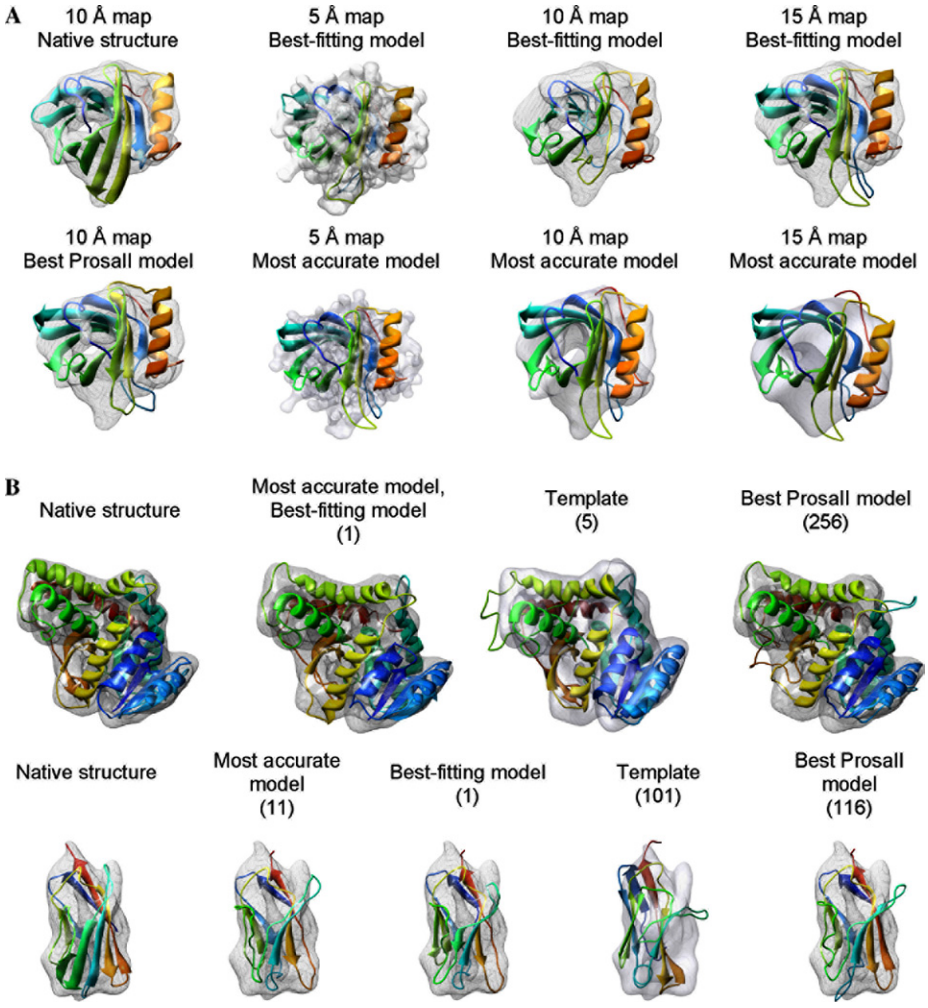

Fig. 4. Examples of optimal fitting of structures into density maps. (A) Fitting of the native structure and models of 1MUP by Mod-EM. The resolutions of the maps without noise and the structures are indicated in the panels. (B) Fitting of the native structures and models of 2CMD and 1CID, as well as their templates (6LDH and 2RHE, respectively) by Mod-EM. The maps are all at 10 Å resolution without noise. The ranking of the models based on the fitting score is indicated in parentheses. The figures were created with the molecular graphics program Chimera (Pettersen et al., 2004).

ProsaII Z-score. Therefore, we explored the possibility of improving the identification of the most accurate model by relying on both the fitting score and the ProsaII Z-score. To combine the two scores for a given model, we first calculated a fitting Z-score by expressing the fitting score relative to the average and standard deviation of the fitting scores for all 300 models of the same protein [$Z_C = (C - \langle C \rangle)/\sigma_C$]. The fitting and ProsaII Z-scores were then added with unit weights to get a combined score. The combined score performed better than either of the two individual scores. The average difference between the RMS errors of the model with the best combined score and the most accurate model dropped below 1 Å at all resolutions. Even at 15 Å resolution, the native overlap was still above 75%. At subnanometer resolutions, the best scoring models were within 0.3 Å RMS error of the most accurate models and had the average native overlap of 82%.

4. Discussion

Our broad objective is to maximize the coverage, accuracy, resolution, and efficiency of structure characterization of protein assemblies (Russell et al., 2004; Sali et al., 2003). This aim will likely be achieved by hybrid methods that consider various types of information, including density maps from cryoEM, atomic structures from crystallography and NMR spectroscopy, and atomic models from protein structure prediction. A major class of such hybrid methods involves the fitting of subunit atomic structures into the cryoEM density map of a large assembly.

In this paper, we combined comparative modeling with the cryoEM fitting. Specifically, we addressed the problem of whether or not simulated cryoEM maps contain enough information to identify the most accurate comparative models among a number of plausible mod-

els based on different alignments between the target sequence and the template structure. We were motivated by the increasing applicability of both cryoEM and comparative modeling. For example, 18 sub-nanometer resolution cryoEM structures of icosahedral particles have been determined recently (Zhou and Chiu, 2003); while the high-resolution structures of their subunits are not known, most of them can be modeled by comparative modeling. Additionally, ~700,000 of the ~1.6 million known protein sequences have at least one domain that can be modeled based on its similarity to one or more of the ~26,000 known protein structures (Pieper et al., 2004). As a consequence, fitting a subunit into a density map is much more likely to involve a comparative model of the subunit than its experimentally determined structure.

Our approach was based on the correlation between model accuracy and the quality of the fit into a density map. Specifically, the method finds an optimal atomic model of a given subunit or domain by fitting alternative comparative models into a given cryoEM map. Alternative models can be calculated by different programs and/or parameter setups, based on different sequence alignments to different template structures. In the present study, the major difference between these alternative models is in the location of deletions as well as in the location and conformation of insertions, given that a comparative model is always almost identical to the template structure in the aligned regions. In principle, such model differences should be detectable at the intermediate cryoEM resolution range (Chiu et al., 2002).

The fitting of a model into a density map was performed either by improved FOLDHUNTER (Jiang et al., 2001) or by a new density fitting module of MODELLER (Mod-EM). Even though the gravity centers of the model and the cryoEM map are approximately overlapping by construction of the benchmark, we used the "scanning Monte Carlo" protocol of Mod-EM to refine both the translational and rotational degrees of freedom (1–2 min per fit). However, a realistic application would involve fitting into cryoEM density maps that are larger than the probe. In such cases, the "scanning Monte Carlo" protocol is not faster than the frequently used correlation-based fitting program FOLDHUNTER (10–15 min per fit), which was also tested here to provide a reference for fitting.

The benchmark clearly demonstrates that the most accurate models can usually be identified by both programs, based on the quality of their fit into the density map, even for noisy maps at 15 Å resolution (Figs. 1–3 and Table 1). Furthermore, these accurate models are fitted with a much higher fitting score than that of the template structure. In other words, an accurate comparative model of a protein based on an experimentally determined atomic structure of a remotely related homolog generally fits better into its density map than the homolog itself. The correlation between the native overlap and the fitting score was dependent on the resolution of the map, resulting in the increased accuracy of the best-fitting models with increasing resolution. For example, at 15 Å resolution, the average native overlap of the model with the highest Mod-EM fitting score was better than 69%, while at sub-nanometer resolution (5–10 Å) this average was above 78%. Both Mod-EM and FOLDHUNTER performed similarly, and we expect that most other fitting programs (Ceulemans and Russell, 2004; Chacon and Wriggers, 2002; Roseman, 2000; Rossmann, 2000; Volkmann and Hanein, 1999; Wriggers et al., 1999; Wu et al., 2003) would also perform comparably. In practice, more than one fitting program may be used on the same problem to increase the confidence in the identified solution.

From the perspective of comparative modeling, the fitting score may be viewed as a model assessment score. There are many model assessment procedures, based on a variety of different considerations (John and Sali, 2003; Melo et al., 2002; Wallner and Elofsson, 2003). Composite scoring that relies on several different criteria is usually most reliable. Therefore, we explored the potential synergy between the fitting score and another model assessment criterion. For this test, we selected the statistical potential *Z*-score calculated by ProsaII (Sippl, 1993), which reflects statistical preferences for the residue solvent accessibilities and pairwise residue distances that were extracted from many known protein structures. Examples of model assessment by both density fitting and statistical potentials reflect the advantage of each method over the other (Fig. 4). Despite the limited size of our benchmark, it is clear that a fitting score is likely to perform better when the alternative models have different shapes (e.g., different loop conformations and lengths) (Fig. 4). Model assessment based on a statistical potential, on the other hand, is expected to perform well when the best model is very accurate and its assessment does not depend on the lack of neighboring subunits. Therefore, the identification of the most accurate model by the fitting score is likely to be improved by consideration of additional model assessment scores.

While our benchmark does indicate the utility of combining comparative modeling with cryoEM fitting into noisy maps at up to 15 Å resolution, the test is not entirely realistic. First, the cryoEM density maps were simulated, not derived from experimental images. Despite our attempt to model the map noise (Fig. 3 and Table 1), the noise in real maps may decrease the observed correlation between the model accuracy and the fitting score. Second, the cryoEM density maps were calculated for the isolated fitted subunits. In practice, the density maps would have to be obtained by segmenting the assembly density, given that cryoEM is currently applied reliably to particles larger than ~150 kDa. This

step could further decrease the correlation between the model accuracy and the fitting score.

Another limitation of our current benchmark is its focus on the errors in the sequence alignment, not in fold assignment and orientations of domains and secondary structure segments. However, such an extended benchmark could easily be created by using different template structures to model the same target sequence and will be explored in the future. Based on the current experience, it is likely that selecting a model with the most accurate fold and secondary structure packing can also be achieved by combined modeling and cryoEM fitting. Moreover, this combined approach could also benefit from additional information, such as the location of long α-helices and large β-sheets, extracted from feature analysis of intermediate resolution cryoEM maps (Chiu et al., 2002; Jiang et al., 2001; Kong and Ma, 2003; Kong et al., 2004).

In summary, we showed that cryoEM density fitting at better than 15 Å resolution can be used as a tool for improving comparative protein structure modeling. Moreover, comparative modeling provides models for fitting into cryoEM maps that are more useful than the experimentally determined structures of the homologs. These results allow for an extension of the hybrid methods by fitting comparative models instead of experimental structures of the homologs into cryoEM density maps. Future directions will involve modifying the alignment, relative orientation of secondary structure segments, and loop conformations during the search for the best fit into a given cryoEM map, by methods such as moulding (John and Sali, 2003), normal mode analysis (Brooks and Karplus, 1983; Go et al., 1983; Levitt et al., 1985; Ming et al., 2002; Tama et al., 2002), and molecular dynamics (Fiser et al., 2000). We will also apply our tools to "real" cryoEM data.

Acknowledgments

We are grateful to Drs. Wen Jiang, Frank Alber, Ben Webb, Andrea Rossi, and Min-Yi Shen for very helpful discussions. This research was supported by NSF (EIA-0325004) and NCRR (P41RR02250). M.L.B. was supported by the NLM (T15 LM07093) through the W.M. Keck Center for Computational Biology of the Gulf Coast Consortia.

References

Alberts, B., 1998. The cell as a collection of protein machines: preparing the next generation of molecular biologists. Cell 92, 291–294.

Baker, D., Sali, A., 2001. Protein structure prediction and structural genomics. Science 294, 93–96.

Beckmann, R., Spahn, C.M., Eswar, N., Helmers, J., Penczek, P.A., Sali, A., Frank, J., Blobel, G., 2001. Architecture of the protein-conducting channel associated with the translating 80S ribosome. Cell 107, 361–372.

Beroukhim, R., Unwin, N., 1995. Three-dimensional location of the main immunogenic region of the acetylcholine receptor. Neuron 15, 323–331.

Bowman, B.R., Baker, M.L., Rixon, F.J., Chiu, W., Quiocho, F.A., 2003. Structure of the herpesvirus major capsid protein. EMBO J. 22, 757–765.

Brooks, B., Karplus, M., 1983. Harmonic dynamics of proteins: normal modes and fluctuations in bovine pancreatic trypsin inhibitor. Proc. Natl. Acad. Sci. USA 80, 6571–6575.

Brünger, A.T., 1992. X-PLOR, Version3.1. A System for X-Ray Crystallography and NMR. Yale Universiy Press, New Haven, CT.

Ceulemans, H., Russell, R.B., 2004. Fast fitting of atomic structures to low-resolution electron density maps by surface overlap maximization. J. Mol. Biol. 338, 783–793.

Chacon, P., Wriggers, W., 2002. Multi-resolution contour-based fitting of macromolecular structures. J. Mol. Biol. 317, 375–384.

Cheng, R.H., Kuhn, R.J., Olson, N.H., Rossmann, M.G., Choi, H.K., Smith, T.J., Baker, T.S., 1995. Nucleocapsid and glycoprotein organization in an enveloped virus. Cell 80, 621–630.

Chiu, W., Baker, M.L., Jiang, W., Zhou, Z.H., 2002. Deriving folds of macromolecular complexes through electron cryomicroscopy and bioinformatics approaches. Curr. Opin. Struct. Biol. 12, 263–269.

Fiser, A., Do, R.K., Sali, A., 2000. Modeling of loops in protein structures. Protein Sci. 9, 1753–1773.

Frank, J., 2002. Single-particle imaging of macromolecules by cryo-electron microscopy. Annu. Rev. Biophys. Biomol. Struct. 31, 303–319.

Gao, H., Sengupta, J., Valle, M., Korostelev, A., Eswar, N., Stagg, S.M., Van Roey, P., Agrawal, R.K., Harvey, S.C., Sali, A., Chapman, M.S., Frank, J., 2003. Study of the structural dynamics of the *E. coli* 70S ribosome using real-space refinement. Cell 113, 789–801.

Go, N., Noguti, T., Nishikawa, T., 1983. Dynamics of a small globular protein in terms of low-frequency vibrational modes. Proc. Natl. Acad. Sci. USA 80, 3696–3700.

Golas, M.M., Sander, B., Will, C.L., Luhrmann, R., Stark, H., 2003. Molecular architecture of the multiprotein splicing factor SF3b. Science 300, 980–984.

Grimes, J.M., Jakana, J., Ghosh, M., Basak, A.K., Roy, P., Chiu, W., Stuart, D.I., Prasad, B.V., 1997. An atomic model of the outer layer of the bluetongue virus core derived from X-ray crystallography and electron cryomicroscopy. Structure 5, 885–893.

Hewat, E.A., Blaas, D., 1996. Structure of a neutralizing antibody bound bivalently to human rhinovirus 2. EMBO J. 15, 1515–1523.

Hewat, E.A., Marlovits, T.C., Blaas, D., 1998. Structure of a neutralizing antibody bound monovalently to human rhinovirus 2. J. Virol. 72, 4396–4402.

Hoenger, A., Sack, S., Thormahlen, M., Marx, A., Muller, J., Gross, H., Mandelkow, E., 1998. Image reconstructions of microtubules decorated with monomeric and dimeric kinesins: comparison with X-ray structure and implications for motility. J. Cell Biol. 141, 419–430.

Jacobson, M., Sali, A., 2004. Comparative protein structure modeling and its applications to drug discovery. Annu. Rev. Med. Chem. 39, 259–276.

Jiang, W., Baker, M.L., Ludtke, S.J., Chiu, W., 2001. Bridging the information gap: computational tools for intermediate resolution structure interpretation. J. Mol. Biol. 308, 1033–1044.

Jiang, W., Li, Z., Zhang, Z., Baker, M.L., Prevelige Jr., P.E., Chiu, W., 2003. Coat protein fold and maturation transition of bacteriophage P22 seen at subnanometer resolutions. Nat. Struct. Biol. 10, 131–135.

John, B., Sali, A., 2003. Comparative protein structure modeling by iterative alignment, model building and model assessment. Nucleic Acids Res. 31, 3982–3992.

Kolatkar, P.R., Bella, J., Olson, N.H., Bator, C.M., Baker, T.S., Rossmann, M.G., 1999. Structural studies of two rhinovirus serotypes complexed with fragments of their cellular receptor. EMBO J. 18, 6249–6259.

Kong, Y., Ma, J., 2003. A structural-informatics approach for mining beta-sheets: locating sheets in intermediate-resolution density maps. J. Mol. Biol. 332, 399–413.

Kong, Y., Zhang, X., Baker, T.S., Ma, J., 2004. A structural-informatics approach for tracing beta-sheets: building pseudo-C(alpha) traces for beta-strands in intermediate-resolution density maps. J. Mol. Biol. 339, 117–130.

Kostyuchenko, V.A., Leiman, P.G., Chipman, P.R., Kanamaru, S., van Raaij, M.J., Arisaka, F., Mesyanzhinov, V.V., Rossmann, M.G., 2003. Three-dimensional structure of bacteriophage T4 baseplate. Nat. Struct. Biol. 10, 688–693.

Levitt, M., Chothia, C., 1976. Structural patterns in globular proteins. Nature 261, 552–558.

Levitt, M., Sander, C., Stern, P.S., 1985. Protein normal-mode dynamics: trypsin inhibitor, crambin, ribonuclease and lysozyme. J. Mol. Biol. 181, 423–447.

Ludtke, S.J., Baldwin, P.R., Chiu, W., 1999. EMAN: semiautomated software for high-resolution single-particle reconstructions. J. Struct. Biol. 128, 82–97.

Ludtke, S.J., Chen, D.H., Song, J.L., Chuang, D.T., Chiu, W., 2004. Seeing GroEL at 6 Å resolution by single particle electron cryomicroscopy. Structure (Camb.) 12, 1129–1136.

MacKerell, J., Bashford, D., Bellott, M., Dunbrack Jr., R.L., Evanseck, J.D., Field, M.J., Fischer, S., Gao, J., Guo, H., Ha, S., Joseph-McCarthy, D., Kuchnir, L., Kuczera, K., Lau, F.T.K., Mattos, C., Michnick, S., Ngo, T., Nguyen, D.T., Prodhom, B., Reiher, I., Roux, B., Schlenkrich, M., Smith, J.C., Stote, R., Straub, J., Watanabe, M., Wiorkiewicz-Kuczera, J., Yin, D., Karplus, M., 1998. All-atom empirical potential for molecular modeling and dynamics studies of proteins. J. Phys. Chem. B 102, 3586–3616.

Mao, Y., Vyas, N.K., Vyas, M.N., Chen, D.H., Ludtke, S.J., Chiu, W., Quiocho, F.A., 2004. Structure of the bifunctional and Golgi-associated formiminotransferase cyclodeaminase octamer. EMBO J. 23, 2963–2971.

Marti-Renom, M.A., Madhusudhan, M.S., Sali, A., 2004. Alignment of protein sequences by their profiles. Protein Sci. 13, 1071–1087.

Marti-Renom, M.A., Stuart, A.C., Fiser, A., Sanchez, R., Melo, F., Sali, A., 2000. Comparative protein structure modeling of genes and genomes. Annu. Rev. Biophys. Biomol. Struct. 29, 291–325.

Melo, F., Sanchez, R., Sali, A., 2002. Statistical potentials for fold assessment. Protein Sci. 11, 430–448.

Metropolis, N., Ulam, S., 1949. The Monte Carlo Method. J. Am. Star. Assoc. 44, 335–341.

Ming, D., Kong, Y., Lambert, M.A., Huang, Z., Ma, J., 2002. How to describe protein motion without amino acid sequence and atomic coordinates. Proc. Natl. Acad. Sci. USA 99, 8620–8625.

Moult, J., Fidelis, K., Zemla, A., Hubbard, T., 2003. Critical assessment of methods of protein structure prediction (CASP)-round V. Proteins 53 (Suppl. 6), 334–339.

Pettersen, E.F., Goddard, T.D., Huang, C.C., Couch, G.S., Greenblatt, D.M., Meng, E.C., Ferrin, T.E., 2004. UCSF chimera—a visualization system for exploratory research and analysis. J. Comput. Chem. 25, 1605–1612.

Pieper, U., Eswar, N., Braberg, H., Madhusudhan, M.S., Davis, F.P., Stuart, A.C., Mirkovic, N., Rossi, A., Marti-Renom, M.A., Fiser, A., Webb, B., Greenblatt, D., Huang, C.C., Ferrin, T.E., Sali, A., 2004. MODBASE, a database of annotated comparative protein structure models, and associated resources. Nucleic Acids Res. 32 (Database issue), D217–D222.

Pittet, J.J., Henn, C., Engel, A., Heymann, J.B., 1999. Visualizing 3D data obtained from microscopy on the Internet. J. Struct. Biol. 125, 123–132.

Rayment, I., Holden, H.M., Whittaker, M., Yohn, C.B., Lorenz, M., Holmes, K.C., Milligan, R.A., 1993. Structure of the actin–myosin complex and its implications for muscle contraction. Science 261, 58–65.

Roseman, A.M., 2000. Docking structures of domains into maps from cryo-electron microscopy using local correlation. Acta Crystallogr. D 56, 1332–1340.

Rossmann, M.G., 2000. Fitting atomic models into electron-microscopy maps. Acta Crystallogr. D Biol. Crystallogr. 56, 1341–1349.

Russell, R.B., Alber, F., Aloy, P., Davis, F.P., Korkin, D., Pichaud, M., Topf, M., Sali, A., 2004. A structural perspective on protein–protein interactions. Curr. Opin. Struct. Biol. 14, 313–324.

Sali, A., Blundell, T.L., 1993. Comparative protein modelling by satisfaction of spatial restraints. J. Mol. Biol. 234, 779–815.

Sali, A., Kuriyan, J., 1999. Challenges at the frontiers of structural biology. Trends Cell Biol. 9, M20–M24.

Sali, A., Glaeser, R., Earnest, T., Baumeister, W., 2003. From words to literature in structural proteomics. Nature 422, 216–225.

Shin, D.S., Pellegrini, L., Daniels, D.S., Yelent, B., Craig, L., Bates, D., Yu, D.S., Shivji, M.K., Hitomi, C., Arvai, A.S., Volkmann, N., Tsuruta, H., Blundell, T.L., Venkitaraman, A.R., Tainer, J.A., 2003. Full-length archaeal Rad51 structure and mutants: mechanisms for RAD51 assembly and control by BRCA2. EMBO J. 22, 4566–4576.

Shindyalov, I.N., Bourne, P.E., 1998. Protein structure alignment by incremental combinatorial extension (CE) of the optimal path. Protein Eng. 11, 739–747.

Sippl, M.J., 1993. Recognition of errors in three-dimensional structures of proteins. Proteins 17, 355–362.

Sosa, H., Dias, D.P., Hoenger, A., Whittaker, M., Wilson-Kubalek, E., Sablin, E., Fletterick, R.J., Vale, R.D., Milligan, R.A., 1997. A model for the microtubule-Ncd motor protein complex obtained by cryo-electron microscopy and image analysis. Cell 90, 217–224.

Spahn, C.M., Beckmann, R., Eswar, N., Penczek, P.A., Sali, A., Blobel, G., Frank, J., 2001. Structure of the 80S ribosome from *Saccharomyces cerevisiae*—tRNA–ribosome and subunit–subunit interactions. Cell 107, 373–386.

Stewart, P.L., Fuller, S.D., Burnett, R.M., 1993. Difference imaging of adenovirus: bridging the resolution gap between X-ray crystallography and electron microscopy. EMBO J. 12, 2589–2599.

Tama, F., Wriggers, W., Brooks 3rd, C.L., 2002. Exploring global distortions of biological macromolecules and assemblies from low-resolution structural information and elastic network theory. J. Mol. Biol. 321, 297–305.

Voges, D., Berendes, R., Burger, A., Demange, P., Baumeister, W., Huber, R., 1994. Three-dimensional structure of membrane-bound annexin V. A correlative electron microscopy-X-ray crystallography study. J. Mol. Biol. 238, 199–213.

Volkmann, N., Hanein, D., 1999. Quantitative fitting of atomic models into observed densities derived by electron microscopy. J. Struct. Biol. 125, 176–184.

Wallner, B., Elofsson, A., 2003. Can correct protein models be identified?. Protein Sci. 12, 1073–1086.

Wang, Y., Rader, A.J., Bahar, I., Jernigan, R.L., 2004. Global Ribosome motions revealed with elastic network model. J. Struct. Biol. 147, 302–314.

Wikoff, W.R., Wang, G., Parrish, C.R., Cheng, R.H., Strassheim, M.L., Baker, T.S., Rossmann, M.G., 1994. The structure of a neutralized virus: canine parvovirus complexed with neutralizing antibody fragment. Structure 2, 595–607.

Wriggers, W., Chacon, P., 2001. Modeling tricks and fitting techniques for multiresolution structures. Structure (Camb.) 9, 779–788.

Wriggers, W., Milligan, R.A., McCammon, J.A., 1999. Situs: A package for docking crystal structures into low-resolution maps from electron microscopy. J. Struct. Biol. 125, 185–195.

Wu, X., Milne, J.L., Borgnia, M.J., Rostapshov, A.V., Subramaniam, S., Brooks, B.R., 2003. A core-weighted fitting method for docking atomic structures into low-resolution maps: application to cryo-electron microscopy. J. Struct. Biol. 141, 63–76.

Zhou, Z.H., Chiu, W., 2003. Determination of icosahedral virus structures by electron cryomicroscopy at subnanometer resolution. Adv. Protein Chem. 64, 93–124.

Zhou, Z.H., Baker, M.L., Jiang, W., Dougherty, M., Jakana, J., Dong, G., Lu, G., Chiu, W., 2001. Electron cryomicroscopy and bioinformatics suggest protein fold models for rice dwarf virus. Nat. Struct. Biol. 8, 868–873.